Experimental Observations of Self-Affine Scaling and Kinetic Roughening at Sub-Micron Lengthscales

Krim, J.; Palasantzas, G.

Published in:
International Journal of Modern Physics B

DOI:
10.1142/S0217979295000239

International Journal of Modern Physics B, Vol. 9, No. 6 (1995) 599–632

EXPERIMENTAL OBSERVATIONS OF SELF-AFFINE SCALING AND KINETIC ROUGHENING AT SUB-MICRON LENGTHSCALES

J. KRIM and G. PALASANTZAS
Physics Department, Northeastern University, Boston, MA 02115

Received 7 September 1994

Experimental observations of self-affine scaling and kinetic roughening at sub-micron length scales are reviewed for thin solid films and ion-beam eroded surfaces.

1. Introduction

A wide variety of surfaces and interfaces occurring in nature are well-represented by a kind of roughness associated with self-affine fractal scaling, defined by Mandelbrot in terms of fractional Brownian motion.[1] Examples of surfaces which exhibit self-affine behavior include the nanometer scale topology of vapor-deposited films,[2] the spatial fluctuations of liquid–gas interfaces,[3] and the kilometer scale structures of mountain terrain.[1] Physical processes which produce such surfaces include fracture,[4] erosion,[5] and Molecular Beam Epitaxy [MBE],[6] as well as fluid invasion of porous media.[7] Whether similar surface morphologies formed by distinctly different physical processes have in fact common basis is a question which remains unanswered. The area of nonequilibrium film growth, and the surface roughness associated with it, shows great promise for illuminating this issue.

Rough film surfaces can occur in both equilibrium and nonequilibrium growth conditions. Films grown under equilibrium conditions are frequently described by one of three basic growth modes, so long as alloying and/or intermixing with the substrate is ruled out[8]: Frank–van der Merwe, Stranski–Krastonov or Volmer–Weber. In the Frank–van der Merwe mode, the film grows in a layer-by-layer fashion, and the surface remains relatively flat throughout the growth process. In the Stranski–Krastonov mode, the film grows in a layer-by-layer fashion up to some limiting thickness, followed by the formation of three-dimensional crystallites. Volmer–Weber growth corresponds to film material condensing directly into the form of three-dimensional crystallites, with no layers forming in advance.

PACS Nos.: 68.55.Jk, 68.35.Bs, 05.40.+j

Solid films grown in far-from-equilibrium conditions are consistently predicted to have self-affine surfaces,[9] and cannot be described by any of these three growth modes. They have been at the intense focus of much recent atomic-scale computer simulation and scaling theory,[10] and although a wealth of theory exists, there are few direct links with experiment. This is partly due to the fact that a precise knowledge of the sample's sub-micron surface topography is required in order to make detailed comparisons with theory. With the advent of new experimental techniques such as scanning probe microscopy,[11] and the adaptation of more longstanding probes such as adsorption[12] and X-ray,[13] electron,[14] and atom-beam[15] scattering, such characterizations have recently become attainable.

We review here the emerging experimental literature reporting self-affine scaling at sub-micron lengthscales for thin solid films and ion-beam eroded surfaces. We provide only a brief outline of the extensive theoretical literature on this topic, and make no mention at all of the massive literature on film growth which falls outside the submicron scaling context. The reader is referred to reviews by Krug and Spohn, and Meakin for extensive discussions of theoretical and computational progress in this area,[10] and to H. A. Atwater *et al.*[16] for a broader treatment of film growth and surface morphology.

2. Self-Affine Surface Roughness

All rough surfaces exhibit perpendicular fluctuations which can be characterized by a mean-square width $\sigma = \langle z(x, y)^2 \rangle^{1/2}$; $z(x, y) = h(x, y) - \langle h(x, y) \rangle$, where $h(x, y)$ is the height function and $\langle \ldots \rangle$ is the spatial average over a planar reference surface. The root-mean-square width does not uniquely define the surface structure: there are many ways to distribute atoms on a surface which will result in the same rms width (Fig. 1). A complete description of surface roughness thus requires knowledge of the lateral roughness (parallel to the interface plane) in addition to that perpendicular to the interface plane. Lateral roughness can be characterized at a very basic level by examining whether the term $z(x, y) - z(x', y')$ is a Gaussian random variable whose distribution depends only on the relative coordinates $(X, Y) \equiv (x' - x, y' - y)$. If so, the roughness is termed "Gaussian". Self-affine roughness is virtually always assumed to be Gaussian. It is characterized by fluctuations in the perpendicular direction $\sigma(L)$ which increase with the horizontal length L sampled as $\sigma(L) \propto L^H$, where $0 < H < 1$ is referred to as the "roughness" exponent.[17] It is also characterized by a height difference correlation function $g(R) = \langle [z(x', y') - z(x, y)]^2 \rangle$; $R = \sqrt{(X^2 + Y^2)}$, which scales as $g(R) \propto R^{2H}$. Actual self-affine surfaces are characterized by an upper horizontal cutoff to scaling, or correlation length ξ, beyond which the surface width no longer scales as L^H, and eventually reaches a saturation value σ. The function $g(R)$ correspondingly saturates to $2\sigma^2$ for $R \gg \xi$.

Figure 1 depicts three self-affine surfaces' profiles which are characterized by different roughness exponents [(a)–(c)], and two surface profiles (one of which is

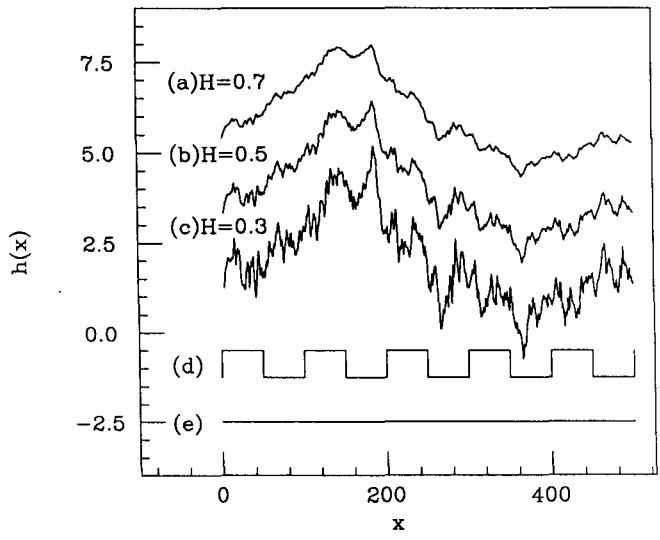

Fig. 1. Profiles of three self-affine surfaces characterized by different roughness exponents (a)–(c), and two surfaces which are not fractal (d)–(e). The self-affine profiles all have the same rms width $\sigma = 1.1 \pm 0.1$. This figure is reproduced from Chiarello *et al.*, Ref. 45.

"rough") which are not fractal [(d), (e)]. The self-affine surface profiles in Fig. 1 all have the same rms width $\sigma = 1.1 \pm 0.1$, so the profile with the smallest roughness exponent is perceived as the "roughest" surface. A decrease in the roughness exponent may in another case appear to correspond to a "smoother" surface. This is because the roughness exponent quantifies how the roughness changes with length scale, and not how the roughness is perceived. It would perhaps be better referred to as a *relative* or *comparative* roughness exponent.[17] Self-affine surfaces can be distinguished from self-similar fractal surfaces by an asymmetry in the scaling behavior perpendicular to the surface, generally manifested by an absence of surface overhangs (Fig. 2).[9] Nonetheless, they are quite commonly assigned a fractal dimension $D = d - H$, where d is the spatial embedding dimension.[1,4] This comes from the fact that horizontal cross-sections of self-affine surfaces consist of "islands" whose "coastlines" are claimed to be self-similar fractals with dimension $D = d - 1 - H$.[18]

The discussion so far has involved only the spatial properties of a rough surface. The time evolution of surface roughness must also be accounted for when considering film growth phenomena. In 1985, Family and Vicsek introduced the notion of "dynamic scaling" in order to incorporate both temporal and spatial scaling behaviors.[19] Within this context, the evolution of the (saturated) rms width with deposition time t is characterized by a "growth" exponent β, according to $\sigma \propto t^{\beta}$. It is assumed here that the film thickness $\langle h \rangle$ is directly proportional to the amount of material deposited and that the deposition rate is constant. The spatial and temporal scaling behaviors of films grown under nonequilibrium conditions can

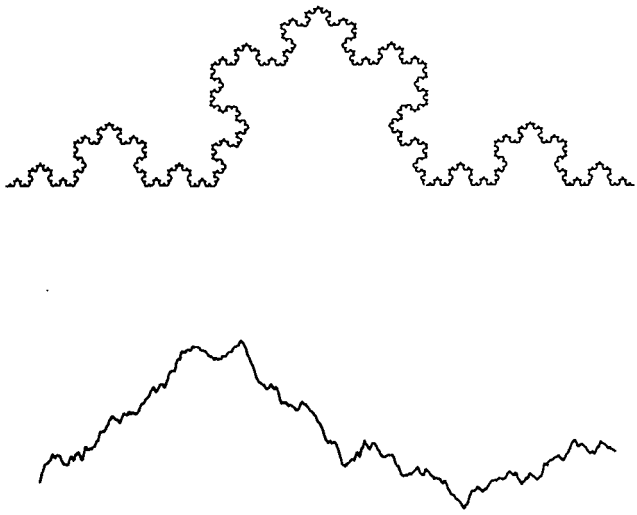

Fig. 2. A self-similar fractal profile with dimension $D = 1.262$ (upper surface) and a self-affine fractal with $H = 0.7$ (lower surface). This figure is reproduced from Panella and Krim, Ref. 68.

then be combined into the dynamic scaling form,

$$\sigma(L, t) = L^H F(t/L^{H/\beta}) \tag{1}$$

where $\sigma(L) \propto L^H$ for $t/L^{H/\beta} \to \infty$ and $\sigma(t) \propto t^\beta$ for $t/L^{H/\beta} \to 0$. Implicit in Eq. (1) is a correlation length which increases with time as $\xi \propto t^{1/z}$, where $z = H/\beta$ is referred to as the "dynamic" scaling exponent. Figure 3 depicts AFM images of the time evolution of electrodeposited copper films which are well-described by Eq. (1). To demonstrate the scaling behavior of the surface, the vertical and horizontal dimensions have been anisotropically scaled in accordance with the spatial and temporal scaling exponents deduced from the quantitative analysis of the surface topology.

Theoretical predictions for the scaling exponents commonly derive from partial differential equations involving phenomenological expansions in the derivatives of a time dependent height function $h(x, y, t)$, describing film growth at a mesoscopic level. Kardar, Parisi and Zhang (KPZ),[20] in a very well-known example of this approach, suggested a continuum equation which does not conserve particle number, and is therefore applicable to cases where desorption and/or vacancy formation, but not surface diffusion, are the dominant surface relaxation mechanisms. Numerous conservative continuum equations have subsequently been proposed,[10] since in many practical situations the dominant surface relaxation mechanism is surface diffusion, with vacancy formation and particle desorption being quite negligible. One widespread example of this is "Molecular Beam Epitaxy" (MBE), where material is slowly evaporated onto the surface of a single crystal at sufficiently high temperature so as to produce a film which bears an epitaxial relation to the substrate.

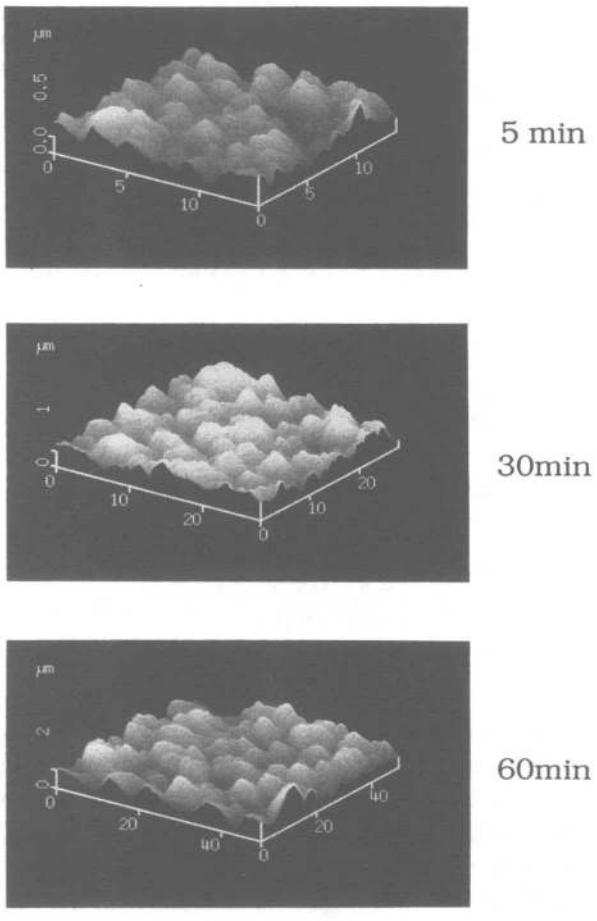

Fig. 3. AFM images of copper surfaces electrodeposited in an acid sulfate solution with an electric current density of 2.4 A/dm^2 for electrodeposition times of (a) 5, (b) 30, and (c) 60 min. To demonstrate the scaling behavior of the surface, the vertical and horizontal dimensions are anisotropically scaled in accordance with the spatial and temporal scaling deduced from the quantitative analysis of the surface height correlations. This figure is reproduced from Iwamoto *et al.*, Ref. 75.

Conservative models have thus also come to be known as "MBE" models, and they predict distinctly different values for the scaling exponents. Measurements of H, β and z are therefore expected to shed light on the atomic-scale origins of particular film morphologies.

Table 1 lists asymptotic values for the scaling exponents associated with growth on a two-dimensional substrate, for selected continuum equations. We note that the theoretical treatment of MBE growth is currently the subject of very lively debate, and the last two equations are listed as representative only. The values quoted for the first and third equations are analytically exact,[21,22] while the values quoted for

Table 1. Asymptotic values for the scaling exponents associated with various continuum equations for nonequilibrium film growth. R_d is the deposition rate, η a "noise" term reflecting spatial and temporal fluctuations in the incoming flux of material, ν and κ_1 are smoothing prefactors reflecting "surface tension", or "surface stiffness" effects, and λ is a "nonlinear" prefactor, reflecting higher growth rates on surfaces with higher slopes.

Model	Equation	(H, β, z)
Edwards–Wilkinson[21,22]	$\frac{\partial h}{\partial t} = R_d + \eta + \nu\nabla^2 h$	$(0, 0, 2)$
KPZ[22,23]	$\frac{\partial h}{\partial t} = R_d + \eta + \nu\nabla^2 h + \frac{\lambda}{2}(\nabla h)^2$	$(0.385, 0.240, 1.61)$
"pure diffusion"[22]	$\frac{\partial h}{\partial t} = R_d + \eta - \kappa_1(\nabla^4 h)$	$(1, 1/4, 4)$
MBE[22,24]	$\frac{\partial h}{\partial t} = R_d + \eta - \kappa_1(\nabla^4 h) + \kappa_2\nabla^2[\nabla h]^2$	$(2/3, 1/5, 10/3)$
MBE[26]	$\frac{\partial h}{\partial t} = R_d + \eta - \kappa_1\nabla^4 h + \nabla[\nabla h f((\nabla h)^2)]$	$f(0) = \nu > 0$, $(0, 0, 2)$
	$\frac{\partial h}{\partial t} = R_d + \eta - \kappa_1\nabla^4 h + \nabla[\nabla h f((\nabla h)^2)]$	$f(0) = \nu < 0$, (1, 1/4-1/3, 3-4)

the KPZ equation have been determined numerically.[23] The values quoted for the fourth equation[22,24] are somewhat under discussion: numerical simulations associated with this equation have in some cases yielded the KPZ values.[25] The fifth equation reduces to the Edwards–Wilkinson equation for cases where no barrier (or a negative barrier) is present for diffusion over a step edge. It yields $H = 1$ and $\beta = 0.25 - 0.33$ for cases where a positive barrier is present for diffusion over a step edge.[26] In the strictest sense, $H = 1$ does not correspond to a self-affine surface. It is regularly associated with the presence of "growth instabilities", large pyramid or moundlike structures which are of uniform size rather than occurring on all lengthscales.[15,27] Figure 4 displays STM images of such pyramid-like structures, which form when positive barriers to edge diffusion are present.

3. Experimental Techniques

Scanning Tunneling Microscopy (STM) and X-ray reflectivity are the experimental techniques which have most commonly been employed for sub-micron characterizations of surface scaling behaviors. The techniques of gas adsorption, Atomic Force Microscopy (AFM), Reflection High-Energy Electron Diffraction (RHEED), High Resolution Low Energy Diffraction (HRLEED), Scanning Electron Microscopy (SEM), Transmission Electron Microscopy (TEM) and helium atom scattering have also been utilized. Not all samples are suitable for all techniques. The various scattering techniques must be carried out on relatively smooth surfaces in order to

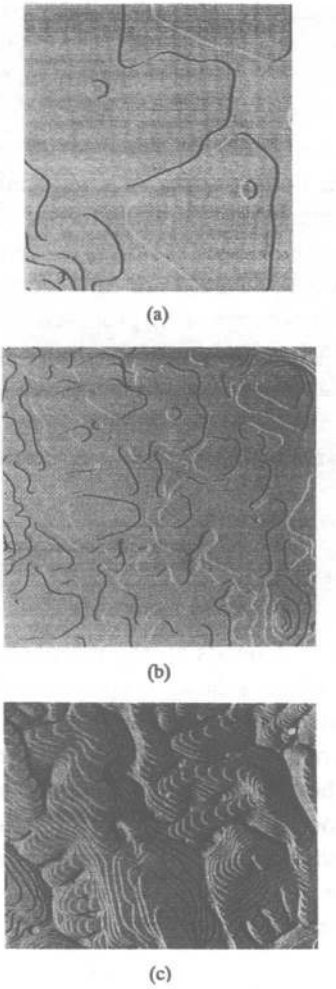

Fig. 4. STM images of homoepitaxial growth of Ag/Ag(111) at room temperature. Nominal film thicknesses: (a) 0.6, (b) 2.7, and (c) 25 monolayers. Fields of view: (a) 7500 × 7500, (b) 11000 × 11000, and (c) 11000 × 9500 Å^2. This figure is reproduced from Vrijmoeth *et al.*, Ref. 71.

minimize beam attenuation effects, and the electron and atom scattering techniques require high vacuum conditions as well. Not all techniques yield values for both scaling exponents: RHEED and TEM provide values for β, while gas adsorption can only probe H. In this section, we summarize the various experimental approaches to the measurement of the static and dynamic scaling exponents.

3.1. *Gas adsorption*

Adsorption was first suggested as a probe of fractal scaling properties by Pfeifer and Avnir in 1983.[28] It is unsurpassed for revealing surface area and porosity of the outer

surface topology at truly atomic length scales, and thus holds promise as a sensitive probe of D or H. Since surface area cannot be directly mapped to rms width, it does not appear to probe the parameter β. Pfeifer and Avnir's original "molecular tiling" approach involved measurement of monolayer adsorption quantities for a range of different adsorbate gases. Under ideal conditions, the number of adsorbate particles N_m with radius a needed to cover a self-similar fractal surface scales as $N_m \propto a^{-D}$, allowing the determination of the fractal dimension D of a substrate.

This original approach, while beautiful in its conception, is limited by a number of experimental constraints,[29] and does not directly address the case of self-affine fractal scaling. An alternative approach, proposed by de Gennes in 1985,[30] and independently by Pfeifer *et al.* in 1989,[12] involves monitoring the number of particles required to cover a surface as it is progressively smoothed by a thickening adsorbate layer. It is an adaptation of the "Frenkel–Halsey–Hill" (FHH) expression[31] for films which completely wet planar substrates to the case of adsorption on a fractally rough surface:

$$\ln(P/P_o) = -\frac{\alpha}{k_B T \theta^n}\,. \tag{2}$$

The coefficient α reflects both the substrate–adsorbate and adsorbate–adsorbate van der Waals interactions,[32] T is the temperature, θ is the quantity of adsorbed material, and the exponent n depends on the morphology of the substrate. Figure 5 presents an STM image[2] of the e-beam evaporated silver sample upon which the Pfeifer *et al.* adsorption data were recorded.[12]

The exact dependence of n on either D (for self-similar substrates) or H (for self-affine substrates), has been the subject of a lively debate,[33–39] which is spurred by the fact that little is known about liquid surface tension at atomic length scales. Apart from the issue of whether or not surface tension is a dominant effect, a consensus does exist for the high coverage (thick adsorbate film) forms of $D(n)$ and $H(n)$.[33–38] If surface tension effects are negligible, then for self-similar,[12,30,38]

$$D = 3\left(1 - \frac{1}{n}\right), \tag{3a}$$

and for self-affine,[33,38]

$$n = 3\,, \tag{3b}$$

while, if such effects are dominant, then for self-similar,[33–38]

$$D = 3 - \frac{1}{n}\,, \tag{3c}$$

and for self-affine,[33,38]

$$H = \frac{2}{n+1} \quad (H > 0.5)\,; \quad n = 3 \quad (H < 0.5)\,, \tag{3d}$$

where the value $H = 0.5$ which divides the regimes in Eq. (3d) pertains to non-retarded van der Waals forces.

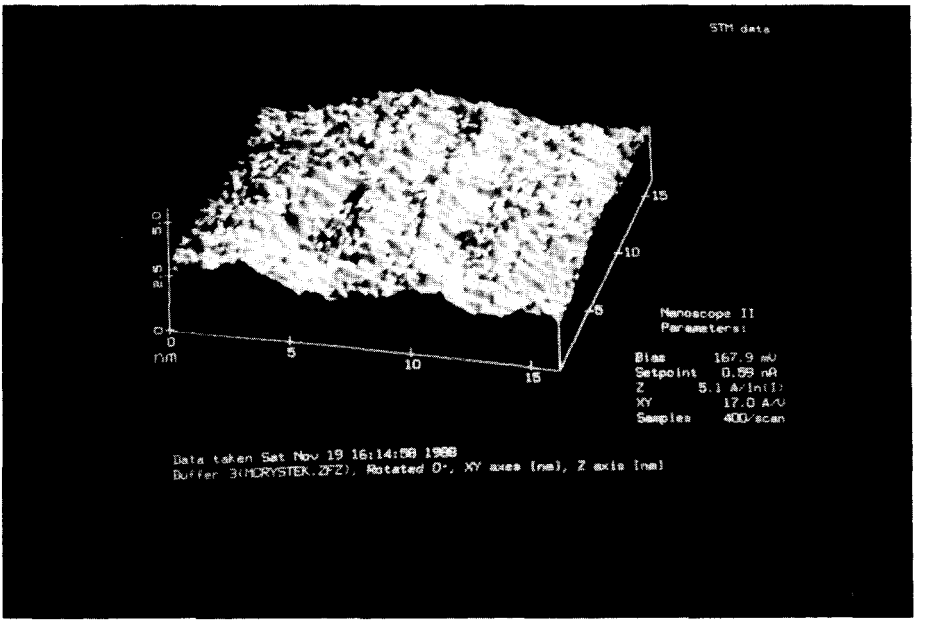

Fig. 5. STM image of a commercially prepared silver film which has been *e*-beam evaporated at room temperature onto the surface of a mechanically polished quartz crystal. This figure is reproduced from Krim *et al.*, Ref. 2.

Adsorption yields ambiguous values for D and H, and does not clearly distinguish between self-affine and self-similar scaling. Future theoretical developments may however allow for more quantitative information to be obtained. Adsorption meanwhile remains a very powerful technique when used in conjunction with experimental probes such as STM or X-ray reflectivity, neither of which can directly detect atomic-scale surface porosity.

3.2. *X-Ray reflectivity*

The specular (angle of incidence equal to angle of reflection) reflection of X-rays from surfaces yields information about the (saturated) rms surface width and also the film density distribution.[13,40–43] X-ray reflectivity measurements usually probe the entire macroscopic extent of the sample, with a typical beam coherence length of ~ 1000 nm. Such measurements virtually always involve samples with coherence lengths well below this value and also with relatively low rms widths, since surfaces with $\sigma \approx 5$ nm or more will substantially attenuate the beam. In practice, this places an upper limit on the film thickness which can be studied, since the thicker films have the larger rms widths.

Specular reflectivity measurements involve recording the scattered intensity as a function of $q_z = \frac{4\pi}{\lambda}\sin(\theta)$, where q_z is the wavevector transfer perpendicular to the surface.[13,40] The data are generally fit by employing a longstanding analysis

approach which is based on a homogenous stratified layer theory,[41–43] where layer thickness, interfacial (Gaussian) widths (σ) and electron densities associated with each layer are the fitting parameters. The fitted data can yield a highly accurate value for the scaling exponent β (Figs. 6 and 13).

Diffuse (angle of incidence not equal to the angle of reflection) X-ray scattering was proposed by Sinha *et al.* in 1988 as a probe of the parameters H and ξ for self-affine surfaces.[13] Sinha *et al.* used perturbation theory on the exact solution of the wave equation for a smooth surface to calculate the diffuse scattering produced by a self-affine surface with a finite horizontal cutoff to scaling. Their expressions for the diffuse scattering,[44] integrated with respect to one direction perpendicular to the scattering plane (X-ray reflectivity data are typically recorded with a slit instead of a pinhole geometry.[45–47]) are given as

$$I(q_x, q_z) = I_0 \frac{\Delta\Omega}{A}(L_x L_y)\frac{|k_0^2(1-n^2)|^2}{16\pi^2}|T(\mathbf{k}_1)|^2|T(\mathbf{k}_2)|^2 S(q_x) \tag{4a}$$

$$S(q_x, q_z) = \frac{\exp(-[(q_z^t)^2 + (q_z^{t*})^2]\sigma^2/2)}{|q_z^t|^2}\int_0^\infty (e^{|q_z^t|^2 C(X)} - 1)\cos(q_x X)dX\,. \tag{4b}$$

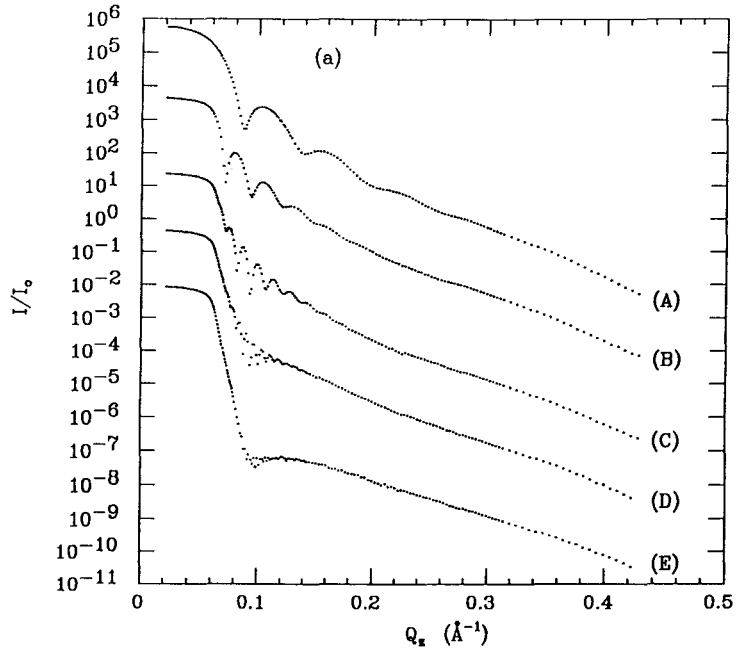

Fig. 6. (a) Specular X-ray reflectivity data for progressively thicker Ag films which have been evaporated at room temperature onto a silicon substrate. (A) 9.8 nm, (B) 18 nm, (C) 36.7 nm, (D) 72.8 nm, (E) 150.2 nm. (b) Fits (solid lines) to the specular reflectivity data. This inset depicts a log–log plot of the rms width σ vs film thickness, with slope $\beta = 0.26 \pm 0.05$. This figure is reproduced from Thompson *et al.*, Ref. 49.

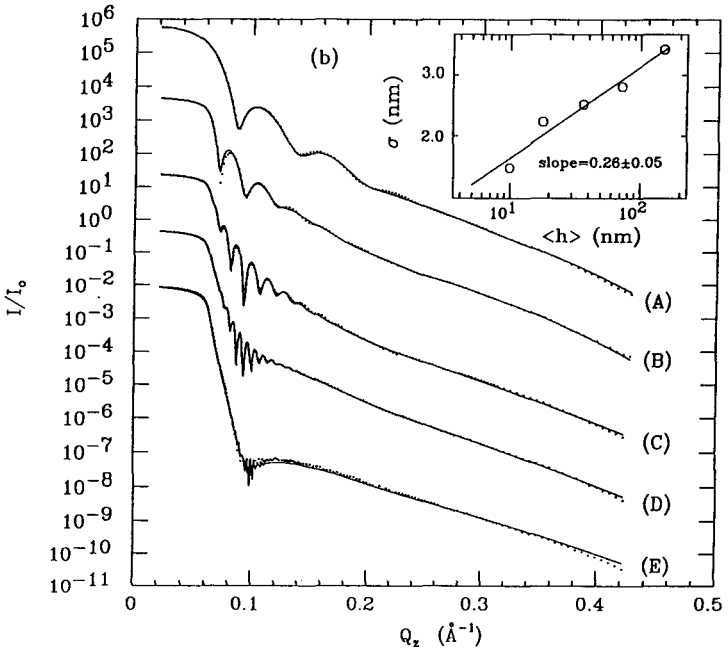

Fig. 6. (*Continued*)

The terms $\mathbf{k}_1$ and $(\mathbf{k}_2)$ are the incident and reflected wavevectors, k_0 the wavevector magnitude, q_x, and q_z^t the in-plane x-component and in-medium z-component of the wavevector transfer, $T(\mathbf{k})$ the Fresnel transmission coefficient, n the index of refraction, L_xL_y the area illuminated by the beam, I_0 and A the intensity and cross-sectional area of the beam, and $\Delta\Omega$ the solid angle subtended by the detector at the sample.

The self-affine nature of a surface enters into Eq. (4b) via the height–height correlation function, $C(R) = \langle z(R)z(0)\rangle = \sigma^2 - g(R)/2$, an explicit form of which much be assumed in order to carry out the data fit. Sinha *et al.* suggested the form $C(R) = \sigma^2 e^{-(R/\xi)^{2H}}$,[13] which incorporates a finite horizontal cutoff to scaling, and provides a quantitative definition for the correlation length ξ as well. This form for $C(R)$ provides an acceptable description of actual correlation data.[48]

The roughness exponent H would ideally be determined from the dependence of the diffuse intensity at specular condition on q_z. However, since there are both specular and diffuse contributions to the scattering intensity recorded at specular condition, the sample in practice is offset slightly from the specular condition to remove the specular component. The diffuse cross-section (recorded at specular condition) of a self-affine surface with no cutoff [Eqs. (4) with $\xi = \infty$ and $q_x = 0$] has the asymptotic form[49]

$$I(q_z) \propto (L_xL_y)\sigma^{-2/H} q_z^{-[2+(1/H)]}, \tag{5a}$$

or

$$I(q_z) \propto \sigma^{-2/H} q_z^{-(3+1/H)}, \tag{5b}$$

depending on whether the area illuminated by the beam is constant (5a) or changes (5b: $(L_x L_y) \propto q_z^{-1}$) as the data are recorded. Numerical calculations reveal this asymptotic form to hold also when the horizontal cutoff is taken into account.[48]

Correlation lengths ξ are determined from fits to diffuse scattering data recorded in a "rocking curve" geometry. In this geometry, the detector is held at a fixed angle, and the sample is rocked about the specular condition in such a way that $\theta_{\text{in}} + \theta_{\text{out}} =$ const. The central maximum in the intensity I_s for such a scan corresponds to the specular condition $\theta_{\text{in}} = \theta_{\text{out}}$. For many common experimental geometries, a rocking curve will only yield accurate values for ξ if the sample correlation length exceeds $\approx 100\,\text{nm}$.[49] Such correlation lengths are usually expected only for relatively thick film samples.

The above discussion of diffuse scattering is based on a single-interface theory. It is thus directly applicable only in cases where the film growth occurs on a substrate whose electron density is equal to that of the deposited material, or to ion beam erosion, where there is no lower interface. For cases where the scattering from the lower interface must also be accounted for, the analysis must in principle be altered to incorporate the presence of multiple interfaces. A formalism for diffuse scattering from a double interface has recently been presented,[50] and a more extensive formalism for multiple interfaces is currently under development.[51] At present, it appears that a single-interface formalism provides a lower bound to the actual value of H.[49]

The difficulties associated with the analysis of scattering data from multiple interfaces are a direct result of the fact that X-rays probe not only the surface, but internal interfaces and film densities as well. Overall this is an asset, since most experimental techniques probe only the outer surface morphology.

3.3. *Electron scattering*

Reflection High Energy Diffraction (RHEED) involves surface scattering of high energy ($\approx 10\,\text{kev}$) electrons, and is highly sensitive to the details of how the sample is terminated.[52] This sensitivity has long been exploited to study layer-by-layer epitaxial growth, which produces temporal oscillations in scattering far from the Bragg reflection angles. Surface roughness, regardless of its origin, also has a strong effect on the modulation of RHEED streaks located at the position of the bulk Bragg peaks. The full width at half maximum (FWHM) of broadened Bragg peaks is closely related to the inverse of the apparent size of the diffracting object,[53] which in this case is the vertical roughness amplitude $\sim \sigma_o$. Measurement of the FWHM thus allows one to estimate σ_o, which is approximately equal to σ, allowing determination of the exponent β.

Both RHEED and low energy electron diffraction (LEED) are relatively insensitive to lateral surface roughness. This is due to the fact that the electron beams employed by these techniques tend to deviate from the ideal case of a monochro-

matic plane wave. Each is a mixture of waves of slightly different energy (energetic width) and direction (angular spread of the beam). The coherence length is on the order of 10 nm for LEED, and only slightly better for RHEED. Lateral resolution on the order of several hundred nm is however attainable via the high resolution detecting techniques of HRLEED,[54] which is capable of probing both H and β.

Yang *et al.* extended the formalism developed by Sinha *et al.*,[13] for x-ray scattering from a continuously rough surface to the case of an atomically stepped surface, (commonly present in MBE) and applied it to the specific case of HRLEED.[14] They obtained the following expression for the time-invariant structure factor associated with diffraction from a surface with atomic steps of height a_0[55]:

$$S(q_{xy}, q_z, t) \sim (([\phi]^{-1/H}\eta)^2 F(q_{xy}[\phi]^{-1/H}n) \qquad \Delta \gg 1 \tag{6a}$$

$$F(y) = \int_0^\infty x e^{-x^{2H}} J_o(yx)dx\,. \tag{6b}$$

The terms q_{xy} and q_z are respectively the in-plane and perpendicular components of the wavevector transfer, $\eta = \xi\sigma^{-1/H}$ is interpreted as the average terrace size, $\Delta = [\phi]^2\sigma^2$, where $[\phi]$ is the modulo 2π of $\phi = q_z a_o$ such that $-\pi \leq [\phi] \leq \pi$, and J_0 is the zeroth-order Bessel function (Fig. 7).

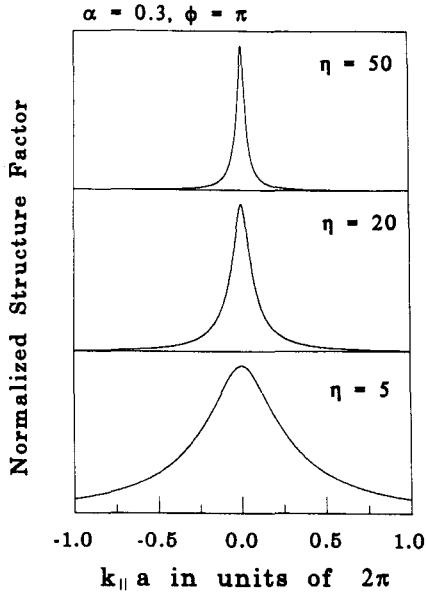

Fig. 7. Line shapes for the structure factor, Eq. (6), associated with scattering from an atomatically-stepped surface. The curves are plotted at the out-of-phase condition, $\phi = \pi$ for different average terrace sizes, $\eta = 5$, 20, and 50 (in units of the lattice constant a_0). The roughness exponent is assumed to be 0.3. This figure is reproduced from Yang *et al.*, Ref. 14.

The value for H is obtained by measuring either the FWHM of the diffraction line shape or the peak intensity [$\propto S(0, q_z)$] as a function of [ϕ], since according to Eq. (6),

$$S(0, q_z) \propto [\phi]^{-2/H} \qquad FWHM \propto [\phi]^{1/H} . \tag{7}$$

The growth exponent β is obtained from the thickness dependence of the the integrated peak intensity R_i in the limit $\Delta \ll 1$, which has the form $R_i \propto e^{-\sigma^2[\phi]^2}$. The reader is referred to Yang, Wang and Lu[56] for a more detailed discussion, including a general overview of scattering techniques as probes of surface roughness.

3.4. *Atom scattering*

Helium atom scattering is a highly surface-sensitive technique where scattering from terraces and step edges are readily distinguishable.[57] Coherence lengths for He beams are on the order of 100 nm,[58] so both lateral and out-of-plane roughness can be probed. Helium atoms have a very large cross-section for scattering from step edges, which leads to additional features in the scattering pattern which would not be resolved in corresponding X-rays or electron-scattering experiments. The statistics of step–step correlations can therefore be studied in addition to the height–height surface correlations. The scattering from the terraces can be analyzed according to the formalism developed by Yang *et al.*,[14] yielding values for both H and β.

3.5. *Scanning probe microscopy*

With the advent of the STM and the AFM in the 1980's,[11] the capability of obtaining accurate topographs at nanometer length scales on both conducting and non-conducting surfaces became a reality. Notwithstanding complications due to surface overhangs and/or tip curvature effects,[59] STM and AFM can be sensitive probes of surface topology over many orders of magnitude. Although a single image yields only local information on surface morphology, the ability to change scan heads allows STM or AFM characterizations of scaling to be carried out over 5 or more orders of magnitude in both lateral and vertical extent.[5] This is a far greater range than is available to alternative techniques such as scattering or adsorption. Characterization of surface topographs in terms of self-affine fractal geometry was first discussed by Mitchell and Bonnell,[4] who employed a power spectrum analysis. Analyses involving variational approaches,[60] height difference correlation functions, and direct rms width versus scan size measurements have also been employed.[5,61,62] In all cases the analysis begins with the recording of topographs $z(x, y)$ for an $L \times L$ area consisting of $N \times N$ points.

The power spectrum approach originally described by Mitchell and Bonnell[4] goes as follows: surface profiles recorded in the fast scan direction are Fourier-analyzed and the coefficients for the individual profiles are then averaged. If a log–log plot of the integrated power spectrum (a log–log plot of the sum from k to ∞ of the squared Fourier amplitudes versus k, where k is the wavenumber) is a straight line, then the

sample is considered self-affine, and the slope of the line will be $-2H$.[63] Mitchell and Bonnell reported that in order for this approach to be accurate, topographs with at least 1000–2000 points/line were required.

Another analysis approach involving relatively few topographs consists of a direct computation of $g(R)$ from the surface profiles. If the surface is self-affine, then a log–log plot of this function versus R will have slope $-2H$. This approach is particularly amenable to cases where the range of scaling is limited, with the lower limit to scaling falling above or near to L/N and the correlation length $\xi \ll L$.

A very direct approach which is neither limited by point density nor sample characteristics is to record many images at different scan sizes, noting the dependence of the rms width on scan size (Fig. 8).[5] A variation of this approach, which is limited by point density but requires only a single image, is to examine the dependence of the width of sub-regions of the image on the length scale examined (Fig. 9). The capability of the latter approach has been tested by analyzing a 256 by 256 square grid using the successive random addition algorithm, and it was found that the roughness exponent is underestimated by 5–20% for $H > 0.6$.[62] The data presented in Fig. 9 are therefore associated with $H = 0.89$, even though the slope of the log–log plot is ≈ 0.7.

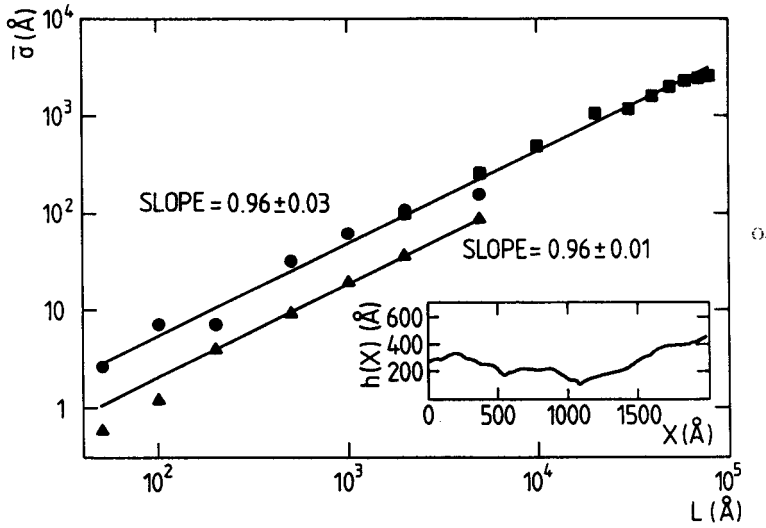

Fig. 8. Average rms width $\bar{\sigma}$ vs scan size L of STM images recorded on a gold film evaporated onto the surface of a mechanically polished quartz crystal. Data represented by circles were recorded in air with various scan heads. Data represented by squares were recorded in vacuum with a second instrument. Each point represents an average of 5–10 scans recorded at random locations. The discrepancy in the absolute value of the data sets is attributed to a calibration discrepancy between the two instruments. The solid lines are least-squares fits to the data. Their slope yields a roughness exponent of 0.96 ± 0.02. Inset: A vertical profile $h(x)$ recorded on the sample. This figure is reproduced from Krim *et al.*, Ref. 5.

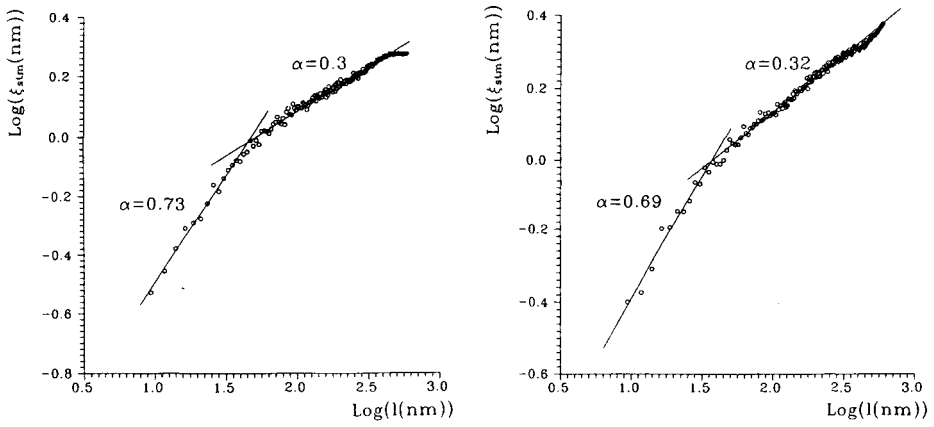

Fig. 9. Rms width ξ vs scale length obtained from a single STM image recorded in a gold film evaporated onto a smooth glass substrate for both the (a) x direction and the (b) y direction. The slopes of the solid lines fit to the x direction yield roughness exponents 0.3 for (horizontal) length scales greater than $\approx$ 40 nm, and 0.89 for length scales less than $\approx$ 40 nm (see text). This figure is reproduced from Salvarezza *et al.*, Ref. 62.

The desirability of a given analysis approach depends on the range of scaling of the particular sample *viz a viz* the scan size analyzed, the grid density of the topograph, and the number of topographs available for averaging. STM cannot be employed for nonconducting surfaces, in which case AFM can be used. The tip-surface distance in the non-contact mode of AFM imaging is however greater than that for STM, with a resulting loss in resolution.

In practice, the determination of β is more problematic for the scanning probe microscopies than the determination of H. This is because the rms width does not effectively saturate until the lateral scan size exceeds many times the sample correlation length, and a scan head capable of probing the relevant length scale may not readily be available. If the saturation value for σ can be established, then β can be directly obtained from its dependence on film thickness.

3.6. *Electron microscopy*

Scanning Electron Microscopy (SEM) is a technique which has long been employed for sub-micron characterizations of surface topology. It involves scanning a focused electron beam (primary energy typically 2–10 keV) over the surface while simultaneously detecting the emitted electrons. The intensity of the emitted signal is associated with variations on the local surface topology of the sample. Under ideal circumstances, the electron beam can be focused to as little as 1 nm.[54]

SEM is generally employed for qualitative, rather than quantitative characterizations of surface morphology, due to the complex nature of the dependence of electron yield on surface chemical and topological properties. It nonetheless has

produced dramatic evidence for scale invariance in a variety of samples, demonstrated by images which appear identical regardless of magnification. The most well-known examples of these are the carbon cauliflower-like structures which have been reported by Messier *et al.*[64]

Quantitative information from SEM can be obtained by studying the cross-section and internal structure of the films if they can be sectioned and/or ion-milled. Fractal scaling properties of specimens are usually determined by polishing, in stages, the surface in the in-plane direction so as to reveal 'islands', and their associated self-similar 'coastlines'. The roughness exponent H is inferred directly from the fractal dimension of these coastlines. Fractal scaling properties can also be probed in a nondestructive fashion by means of a stereoscopic SEM method.[65]

Transmission Electron Microscopy (TEM) involves the use of high energy electrons ($> 50\,\text{keV}$), which are diffracted as they pass through a thin sample and are then focused into an image consisting of a two-dimensional projection of the sample structure. Under ideal circumstances, the image resolution can be as little as 0.2–0.3 nm. Layer structures documenting the evolution of surface roughness can be observed in sufficiently thin ($\approx 100\,\text{nm}$ or less) vertical film slices, by 'marking' the film at regular intervals through deposition of a contrasting element (Fig. 10).[66,67]

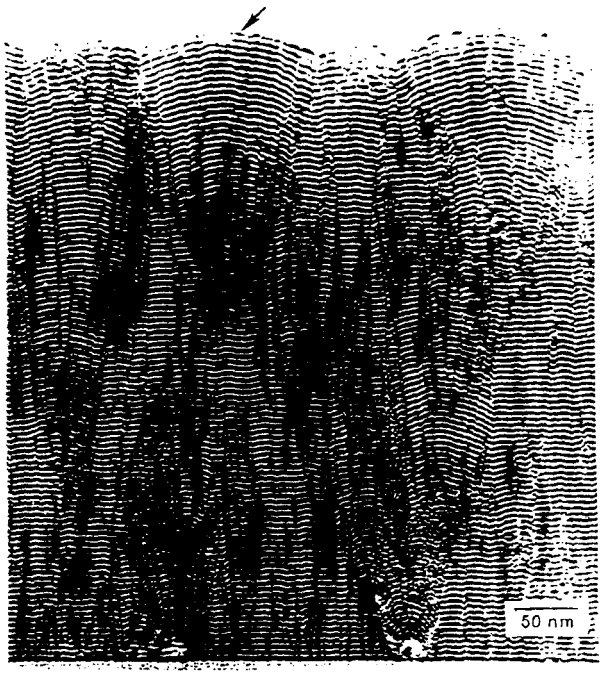

Fig. 10. Sequential cross-section TEM micrograph of a multilayer film which has been thinned to $\approx 40\,\text{nm}$ for electron transparency. The multilayer is comprised of 101 layers of AlN which are 2 nm thick, alternating with 100 layers of NbN which are 3 nm thick. This figure is reproduced from Miller *et al.*, Ref. 66.

4. Thin Solid Film Growth

This section lists experimental reports of sub-micron scaling phenomena for thin solid film growth. Table 2 provides a summary of the information, and includes information on roughness amplitudes as well as the scaling exponents.

Table 2. Summary of Exponents and Amplitudes Reported for Solid Film Growth. T_s is the substrate tempertaure, R_d the deposition rate, P the pressure, θ the deposition angle with respect to the substrate normal, h the film thickness, ξ the correlation length, σ the saturated rms width, H the roughness exponent and β the growth exponent.

Substrate	T_s K	R_d nm/s	P torr	θ deg.	h nm	ξ nm	σ nm	H	β
				Ag					
quartz[45]	80	0.05	10^{-8}	5	110	145	0.85	0.46	
quartz[68]	80	0.03	10^{-7}	5	45-250			fractal	
Si[49]	300	0.03	10^{-7}	0	10-150	< 100	0.5–3.5	0.70	0.26
Ag(111)[71,72]	300	0.004	10^{-10}	0	0.15-6		0.1-0.8	1	
quartz[73]	300	0.03	10^{-8}	0	30-700	15-60	2.2-6.0	0.82	0.29
				Au					
Si(111)[74]	220	0.05	10^{-2}		350	200	3	0.42	
Si(111)[74]	220	0.05	10^{-2}		7-270		0.5-2.5		0.42
glass[4]	300		10^{-1}	0	50			0.74	
glass[62]	300	30	10^{-4}	2-25	30-850	≈ 40	0.7-2.6	0.89	0.41
Si(111)[74]	300	0.05	10^{-2}		10-120		0.6-2.0		0.40
quartz[45]	500	0.05	10^{-9}	0	150	330	2.2	0.95	
quartz[45]	500	0.05	10^{-9}	0	150			not fractal	
				Cu					
Cu(100)[15]	160	0.001	10^{-9}	*	0.5-7.5		0.15-0.3	1	0.26
Cu(100)[15]	160	0.001	10^{-9}	*	2.35	2.2	0.22		
Cu(100)[15]	200	0.001	10^{-9}	*	0.5-11		0.1-0.8	1	0.56
Cu(100)[15]	200	0.001	10^{-9}	*	7.2	10.6	0.72		
Cu[75]	300	8.3			500-30000	10^3	100-700	0.87	0.45
				Si					
Si[67]	573	0.01			5-30		0.2-1.2		1
				Fe					
Si(111)[76]	323	0.01	10^{-10}		0.2-75		0.25-8.5		0.22-0.3
Fe(001)[6]	343	0.01			0.5-0.31	≈ 1.4	0.11-0.16	0.79	0.22
				AlCu and AlSi					
AlCu/Si[47]	473				468	110	1.8	0.7	
AlSi/Si[47]	473				600	400	4.2	1	

Table 2. (*Continued*)

Substrate	T_s K	R_d nm/s	P torr	θ deg.	h nm	ξ nm	σ nm	H	β
				InP					
InP(1000)[77]	773	0.01-0.05			0.1-100		0.05-0.1		0.2
				NbN					
sapphire[66]	573	4			20-500		0.5-1.5		0.27
				CuCl					
CaF_2(111)[78]	353, 383	0.04			6-40	≈ 200	≈ 20	0.84	
				$CH_{1.3}$ Polymer					
Si[79]	318	0.55			30-20,000	20-2000	1-100	0.90	0.7
Si[79]	318	0.41			500-20,000	10^3	1-100	0.95	0.9
Si[79]	318	0.27			1-70, $\times 10^3$10^3		1-100	1.1	1.0
Si[79]	318	0.22			1-8, $\times 10^4$		0.6-2		0.27

*angle varied

4.1. *Pure metals*

4.1.1. *Ag at 80 K*

1991: Chiarello *et al.*[45] thermally evaporated a 110 nm thick Ag/quartz film at 80 K, 0.05 nm/s, 10^{-8} torr and 5° off-normal incidence. The films were warmed to 300 K in the course of an *in situ* transfer to an X-ray analysis chamber. X-ray reflectivity measurements were carried out on the film, yielding $H = 0.46 \pm 0.10$ and $\xi = 145$ nm, according to the single interface analysis approach outlined in Sec. 3. The value for H obtained from this formalism is believed to provide a lower bound to the actual value of H, while the value obtained for ξ should be an upper limit.[48,49] Nitrogen gas adsorption measurements were recorded *in situ* on a silver film prepared in an identical manner, and it was concluded that the sample was either a self-affine or self-similar fractal.[45]

1994: Panella and Krim[68] thermally evaporated 45–250 nm thick Ag/quartz films at 80K, 0.03 nm/s, 10^{-7} torr and both normal and 5° off-normal incidence. The films were warmed to 300 K in the course of an *in situ* transfer to a gas adsorption tip. The films were examined by means of nitrogen gas adsorption at 77 K, and those which were deposited at 5° off normal incidence were observed to have substantially larger surface areas than those deposited at normal incidence. They exhibited either self-affine or self-similar fractal scaling, while the films deposited at normal incidence were planar to within experimental resolution (Fig. 11).

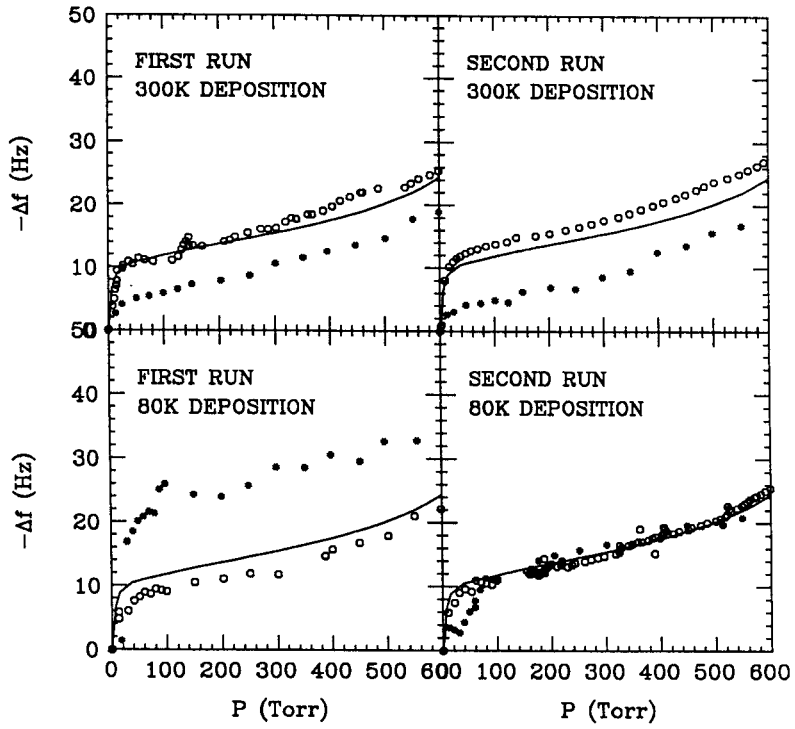

Fig. 11. Low coverage data for liquid nitrogen adsorption at 77 K on 150 nm-thick silver films deposited at 80 K and 300 K onto optically polished quartz substrates. Circles denote silver films deposited at normal incidence. Asterisks denote silver films deposited at 5° off-normal incidence. Solid lines represent the theoretical prediction for adsorption on a flat silver surface. The frequency shift associated with the "knee" of each curve is proportional to the number of nitrogen moelcules required to coat the surface with one monolayer. This figure is reproduced from Panella and Krim, Ref. 68.

4.1.2. *Ag at 300 K*

1989: Pfeifer *et al.*[12] analyzed nitrogen gas adsorption data recorded at 77 K on commercially-prepared, *e*-beam evaporated silver films (Fig. 5).[2] They reported a fractal dimension of 2.3 according to a model which assumed self-similarity rather than self-affinity. Krim and Panella[69] later established that the surface topology was a result of the roughness of the underlying quartz substrate rather than the film deposition conditions. Such samples remain quite useful for the development of theories of adsorption on fractal surfaces.[70]

1994: Thompson *et al.*[49] thermally evaporated 10–150 thick Ag/Si films at 300 K, 0.03 nm/s, 10^{-7} torr and normal incidence. X-ray reflectivity measurements were carried out *in situ*, yielding $H = 0.70 \pm 0.10$, $\xi \leq 100$ nm, and $\beta = 0.26 \pm 0.05$, according to the single interface analysis described in Sec. 3 (Fig. 6). The value for H is believed to be a lower bound to the actual value of H.[48,49]

1994: Panella and Krim[68] thermally evaporated 45–250 nm thick Ag/quartz films at 300 K, 0.03 nm/s, 10^{-7} torr and both normal and 5° off-normal incidence. *In situ* nitrogen adsorption measurements at 77K indicated the films to be planar, within experimental resolution (Fig. 11).

1994: Vrijmoeth *et al.*[71] evaporated 0.15–6 nm thick Ag/Ag(111) films at 300 K, 0.004 nm/s, 10^{-10} torr and normal incidence. They examined the films *in situ* with STM and observed "pyramid-like" structures, which are generally associated with the roughness exponent $H = 1$ (Fig. 4). Heyvaert *et al.*[72] deposited Ag/Ag(111) films in similar conditions, and confirmed the exponent $H \approx 1$ for the film thickness range 3–500 nm.

1994: Palasantzas and Krim[73] thermally evaporated 30–700 nm thick Ag/quartz films at 300 K, 0.03 nm/s, 10^{-7}–10^{-8} torr and normal incidence. They examined the films in a nitrogen environment by means of STM, primarily through analysis of height–height correlation data. They tracked the progression of the coherence length, the rms width and the roughness exponent for two orders of magnitude in film thickness, and obtained independent values for all three scaling exponents. They observed no evolution of the exponents' values with film thickness (Fig. 12), and concluded that the measured values, $H = 0.82 \pm 0.05$, $\beta = 0.29 \pm 0.06$ and $z = 2.53 \pm 0.50$, had reached their asymptotic limits. These values are consistent with relation $z = H/\beta$, but inconsistent with a second relation, $2H = z - 2$, which is thought to be generally applicable for conservative growth on a two-dimensional substrate.[22] Palasantzas and Krim also noted that the coherence length ξ observed for these films was nearly equal to their grain size.

4.1.3. *Au at 220 K*

1993: You *et al.*[74] sputter deposited a 350 nm thick Au/Si(111) film at 220 K in 10 mtorr of Ar at 0.05 nm/s and analyzed the height–height correlations of STM images recorded on the film after it had been warmed to room temperature. They reported $H = 0.42$ and $\xi \approx 200$ nm for this film. They also carried out *in situ* X-ray reflectivity measurements on films deposited in this manner for the thickness range 7–270 nm, and found $\beta = 0.42$, employing the value $H = 0.42$ in their data fitting routines (Fig. 13). You *et al.* employed an analysis approach which was alternate to that outlined in Sec. 3.

4.1.4. *Au at 300 K*

1990: Mitchell and Bonnell[4] sputter deposited a 50 nm thick Au/glass film in $\approx$ 150 mtorr of Ar at normal incidence angle. They examined the film in air by means of STM, and reported $H = 0.76 \pm 0.04$, employing a power spectrum analysis.

1991: Chiarello *et al.*[45] thermally evaporated a 70 nm thick Au/quartz film at 300 K in 10^{-9} torr at 0.05 nm/s. They carried out X-ray reflectivity measurements on the film and concluded the film was not self-affine. The correlation length for this film was determined to be $\xi = 700$ nm. Chiarello *et al.* also carried out *in situ* nitrogen

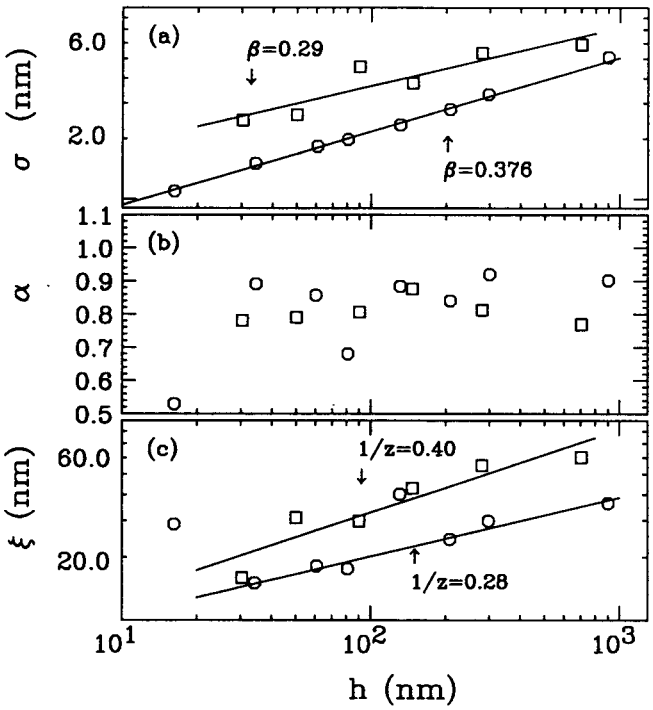

Fig. 12. Thickness dependence of the rms width (a), the roughness exponent (b), and the correlation length ξ (c) for silver films deposited at normal incidence onto optically polished quartz substrates at room temperature. The data represented by squares are the primary results of the study. This figure is reproduced from Palasantzas and Krim, Ref. 73.

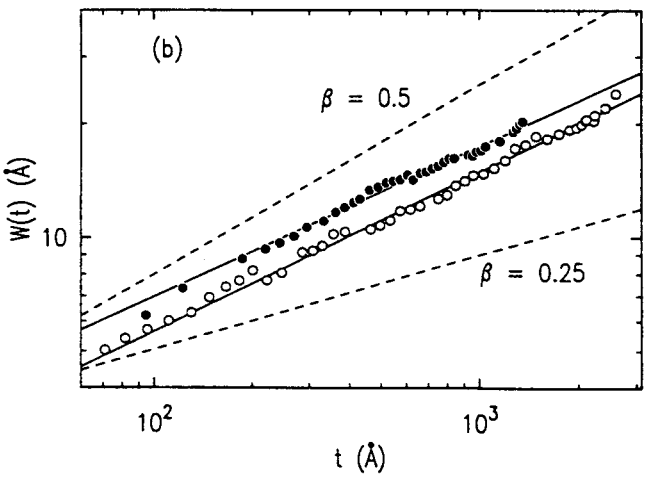

Fig. 13. Rms widths of gold films sputtered onto silicon (111) at 220 K (open circles) and 300 K (filled circles). The widths were determined via fits to specular reflectivity data. The solid lines are the power-law fits to the data, yielding $\beta = 0.42$ and 0.40. The dashed lines ($\beta = 0.25 = 0.5$) are shown for reference. This figure is reprodued from You *et al.*, Ref. 74.

adsorption measurements at 77 K on the same film, which indicated it was planar, within experimental resolution.

1992: Herrasti *et al.*[61] thermally evaporated 30–1000 nm thick Au/glass films at 298 K, 30 nm/s, 10^{-4} torr and incidence angles between 2° and 25° with respect to normal. They examined the films in air by means of STM, and observed height distributions consistent with self-affine rather than self-similar surfaces. Employing a direct rms width versus scan size analysis approach, they reported $H \approx 1/3$ for scan sizes in the range $\approx$ 50–1600 nm. Gold films in the thickness range 30–1200 nm were also deposited electrochemically at 100 nm/s onto a Au electrode in 0.5 M H_2SO_4 solution. The films were examined in air by means of STM, yielding $H = 0.5 \pm 0.1$.

1992: The data reported by Herrasti *et al.*[61] for vapor-deposited films were reanalyzed by Salvarezza *et al.*,[62] who reported $H = 0.89 \pm 0.05$, for (lateral) length-scales below $\approx$ 38 nm, crossing over to $H = 0.35 \pm 0.05$ for length-scales in excess of $\approx$ 38 nm (Fig. 9). (The value of $H = 0.89$ is reported in Table 2 rather than $H = 0.35$, since virtually all of the other experimental reports involve analyses at lateral length scales remaining below $\approx$ 50 nm.) Salvarezza *et al.* did not report a value for β, but Fig. 2 of their publication depicts the saturated rms width versus film thickness, from which a value $\beta = 0.41 \pm 0.06$ can be deduced.

1993: You *et al.*[74] sputter deposited Au/Si(111) films at 300 K in 10 mtorr of Ar at 0.05 nm/s for the film thickness range 10–120 nm. They carried out *in situ* X-ray reflectivity measurements on these films, and found $\beta = 0.40$, employing the value $H = 0.42$ in their data fitting routines (Fig. 13).

4.1.5. *Au at 500 K*

1991: Chiarello *et al.*[45] thermally evaporated a 150 nm thick Au/quartz film at normal incidence, 500 K and 0.05 nm/s and 10^{-9} torr. They carried out X-ray reflectivity measurements on the film and observed $H = 0.95 \pm 0.10$ and $\xi = 330$ nm, employing the analysis approach outlined in Sec. 3. *In situ* nitrogen adsorption measurements at 77 K on the same film indicated it was rough, but not self-affine.

4.1.6. *Cu at 160 K and 200 K*

1994: Ernst *et al.*[15] evaporated 0.5–7.5 nm thick Cu/Cu(100) films at 160 K, 0.001 nm/s, 10^{-9} torr. The incidence angle varied in the course of the deposition. Helium beam scattering measurements were carried out *in situ*, yielding $H \approx 1$ and $\beta = 0.26$ (Fig. 14). The correlation length was reported to be $\xi = 2.2$ nm for a 2.3 nm thick film. They also evaporated 0.5-11 nm thick Cu/Cu(100) films at 200 K, 0.001 nm/s and 10^{-9} torr, and obtained $H \approx 1$ and $\beta = 0.56$. The correlation length was reported to be $\xi = 10.6$ nm for a 7.2 nm thick film. Through analysis of both step and terrace correlations throughout the growth process, they concluded that the initially singular surface was transformed into an arrangement of vicinal surfaces resulting in a pyramidlike surface profile ("unstable growth"). The sides of

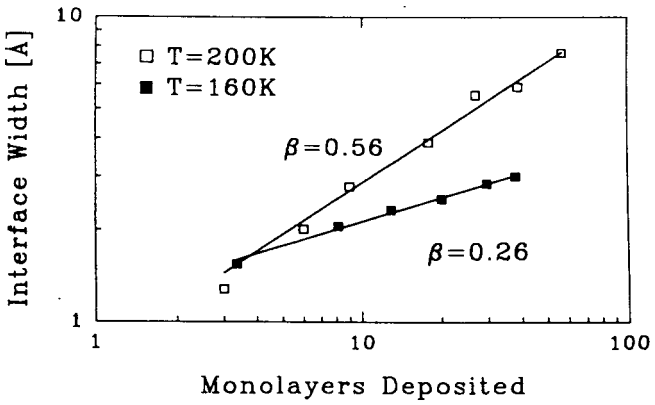

Fig. 14. Rms width of copper films evaporated onto Cu(100) at 160 K (closed squares) and 200 K (open squares). The solid lines are power-law fits to the data, yielding $\beta = 0.26$ and 0.56. This figure is reproduced from Ernst *et al.*, Ref. 15.

the pyramids were composed of the (113) and (115) Cu surfaces for deposition at 160 K and 200 K, respectively.

4.1.7. *Cu at 300 K*

1994: Iwamoto *et al.*[75] electrochemically deposited 500–30000 nm thick Cu films onto a Cu electrode at 300 K and 8.3 nm/s in a stirred $CuSO_4$ solution (Fig. 3). They examined the films in air by means of AFM, employing a direct rms width versus scan size analysis approach, and reported $H = 0.87 \pm 0.05$ and $\beta = 0.45 \pm 0.05$. They observed the same roughness exponent for lower current densities. The morphology was observed to be unstable at higher current densities. Iwamoto *et al.* interpreted the observed scaling behaviors to result from the enhanced growth of protrusions owing to nonlocal Laplacian growth effects.

4.1.8. *Si at ≈ 573 K*

1992: Eaglesham and Gilmer[67] deposited 5–30 nm thick Si films onto Si substrates at ≈ 573 K and 0.01 nm/s. The samples were marked with a sequence of Ge layers dispersed throughout the film, and then were examined by means of TEM. They observed a growth exponent $\beta = 1$, and presented arguments that this anomalously large exponent (i.e. $\beta > 0.5$) could be the result of asymmetric sticking of deposition particles at step edges.

4.1.9. *Fe at ≈ 333 K*

1991: Chevrier *et al.*[76] evaporated .2–75 nm thick Fe/Si(111) films at 323 K, 0.002–0.02 nm/s and 10^{-10} torr. RHEED measurements were carried out *in situ*, yielding $0.22 \leq \beta \leq 0.3$.

1992: He *et al.*[6] evaporated 0.5-31 nm thick Fe/Fe(001) films 343 K, 0.01 nm/s (0.144 nm/layer), 10^{-9} torr and normal incidence. HRLEED measurements were carried out *in situ*, yielding $H = 0.79 \pm 0.05$ and $\beta = 0.22 \pm 0.02$. He *et al.* argued that scaling theories of kinetic growth were definitely applicable to this case of homoepitaxial growth, and interpreted their results as supportive of conservative growth models.

4.2. *Compounds*

1992: Weber and Lengeler,[47] analyzed a 468 nm-thick AlCu/Si film which was thermally evaporated at 473 K. They examined the film in air by means of AFM and X-ray reflectivity, and reported $H = 0.7$ and $\xi = 110$ nm. They also examined a 600 nm thick AlSi/Si film evaporated at 473 K, and reported $H \approx 1$ and $\xi = 400$ nm. Based on their results, they proposed a modification of the distorted-wave Born approximation analysis for diffuse X-ray reflectivity developed by Sinha *et al.*[13]

1992: Miller *et al.*,[66] deposited NbN films on sapphire at 573 K and 4 nm/s. The films were marked at regular intervals with layers of AlN (Fig. 10). They were then sectioned and ion-milled with Ar^+ at 5 keV and 0.8 mA to obtain thin vertical sections for TEM. They obtained $\beta \approx 0.27$ for the film thickness range 20–500 nm.

1993: Cotta *et al.*,[77] evaporated 1–2000 nm thick InP/InP(100) films at 773 K-793 K and 0.01–0.05 nm/s. The samples were examined in air by means of AFM along the $[0\bar{1}\bar{1}]$ and $[0\bar{1}1]$ directions, and a factor of ≈ 3 difference in the rms roughness was observed. For films deposited below 793 K, two power law regimes were reported for the scaling behavior of the roughness in the $[0\bar{1}1]$ direction. The growth exponent $\beta = 0.2$ was observed for the 0.1–100 nm thickness range of a film deposited at 793 K, in the $[0\bar{1}1]$ direction.

1994: Tong *et al.*[78] deposited 6–40 nm thick CuCl films onto $CaF_2(111)$ substrates at 353 K–383 K and 0.04 nm/s. The samples were examined in air with a AFM, and roughness exponents were obtained from the dependence of the interfacial width on the length scale probed, yielding $H = 0.84 \pm 0.054$. Tong *et al.* argued that scaling theories of kinetic growth could be applicable to cases of heteroepitaxy as well as homoepitaxy, and interpreted their results as supportive of conservative growth models.

4.3. *Polymers*

1994: G. W. Collins *et al.* [79] employed an RF plasma discharge technique to deposit polymer films onto silicon substrates at 318 K. The atomic composition of the films was determined by combustion microchemical analysis to by $CH_{1.3}$, and the chemical composition was thought to resemble a highly crosslinked polyethylene. The films were examined in air with AFM, and the exponents were obtained through a power spectrum analysis. They obtained $H = 0.90 \pm 0.07$, $\beta = 0.7$, and $z = 1.4$ for 30–20,000 nm thick films deposited at 0.55 nm/s (Fig. 15), $H = 0.95 \pm 0.07$, $\beta = 0.9$, and $z = 1.1$ for 500–20,000 nm thick films deposited at 0.41 nm/s, $H = 1.1$, $\beta = 1.0$,

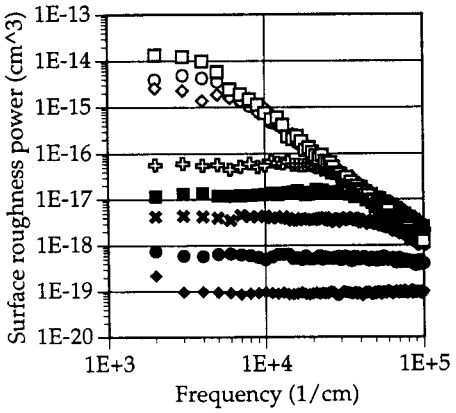

Fig. 15. Evolution of the surface roughness power spectra with increasing film thickness for plasma polymer films deposited at 0.55 nm/s. 19.7 μm (open squares), 11.1 μm (open circles), 8.5 μm (open diamonds), 1.1 μm (+), 0.53 μm (filled squares), 0.28 μm (x), 0.14 μm (filled circles), 0.07 μm (filled diamonds). This figure is reproduced from Collins *et al.*, Ref. 79.

and $z = 1$ for 1000–70,000 nm thick films deposited at 0.27 nm/s, and $\beta \approx 0.27$ for 10,000–80,000 nm thick films deposited at 0.22 nm/s. Collins *et al.* argued that scaling theories of kinetic growth could be applicable to cases of polymer growth, despite the fact that the deposited particles were intertwined, and interpreted their results as supportive of conservative growth models.

5. Erosion and Other Studies

The sub-micron topology of a surface produced by ion bombardment or erosion has received far less theoretical attention than that of a vapor-deposited film.[80] The scaling theories applicable to nonequilibrium film growth might however be applicable to cases of erosion, if no material is redeposited onto the surface during the erosion process.[81] If so, the topography of a film deposited onto an initially smooth substrate would be quite similar to that of an initially smooth surface which is subjected to ion-bombardment: a self-affine fractal surface is expected to develop, and its rms width should exhibit a power law dependence on time. Experimental reports of sub-micron scaling phenomena for cases of surface erosion are listed in this section, and summarized in Table 3. We also mention here of a case involving the evolution of surface roughness due to time-dependent rearrangement of material at the surface rather than its addition or removal.

5.1. *Ion-beam erosion*

5.1.1. *Graphite*

1991: Eklund *et al.*,[82] exposed the (0001) surface of highly-oriented pyrolytic graphite to 5 keV Ar^+ ions at an angle of 60° with respect to substrate normal.

Table 3. Summary of Exponents and Amplitudes Reported for Ion Beam Erosion T_s is the substrate temperature, R_d the flux (which is proportional to the material removal rate) θ the sputtering angle with respect to the substrate normal, h the fluence (which is proportional to the amount removed), ξ the correlation length, σ the saturated rms width, H the roughness exponent and β the growth exponent.

ion	energy keV	T_s K	R_d ions/(cm^{2}s)	θ deg.	h ions/cm^2	ξ nm	σ nm	H	β
			Graphite (0001)						
Ar^+ [82]	5	300	6.9×10^{13}	60	10^{16}–10^{17}	10–20		0.2–0.4	
Ar^+ [82]	5	600	3.5×10^{14}	60	10^{17}	10–20		1	
			Fe(100)						
Ar^+ [5]	5	300	5×10^{14}	25	10^{17}–10^{18}	> 100		0.53	
			SiO_2						
Xe[83]	1	300	3.3×10^{12}	55	10^{14}–10^{16}		0.3–0.8		1
			Ge						
Xe[84]	1	623	3×10^{12}	55	10^{15}–10^{16}		0.1–0.25		< 1

Substrates held at 300 K were exposed to fluxes of 6.9×10^{13} and 3.5×10^{14} ions/(cm^{2}s) for time periods corresponding to fluences of 10^{16}, 10^{17}, and 10^{18} ions/cm^2, or $\approx$ 10–1000 monolayers of material removed (Fig. 16). Substrates held at 600 K and 900 K were exposed to a fluxes of 3.5×10^{14} ions/(cm^{2}s) for time periods corresponding to fluences of 10^{17} ions/cm^2, or $\approx$ 100 monolayers of material removed. The samples were examined in air with an STM, and exponents were obtained via a power spectrum analysis. A roughness exponent of $0.2 \leq H \leq 0.4$ was observed for the 300 K substrate, for the lower flux at the two lowest fluences (Fig. 16(a) and (b)). Correlation lengths, on the order of 10–20 nm, were observed to increase with fluence, with a dynamic exponent z in the range 1.6–1.8. Surface widths were observed to increase with both flux and fluence, but no value for the growth exponent β was reported. A roughness exponent of $H \approx 1$ was observed for the data recorded at 600 K.

5.1.2. *Fe*

1993: Krim *et al.*[5] studied the erosion of Fe(100) films sputtered with 5 keV Ar^+ ions. The Fe(100) surface was obtained by depositing 200 nm of Fe on MgO(001) at 150°C, followed by annealing to 600° C. The surfaces were bombarded at an angle 25° with respect to normal with a flux of 5×10^{14} ions/cm^2*s*, and fluences ranging from 10^{17}–10^{18} ions/cm^2. The samples were studied *in situ* with STM and roughness exponents were obtained from the dependence of the rms width on scan size. A roughness exponent $H = 0.53 \pm 0.02$ was observed, independent of ion flux.

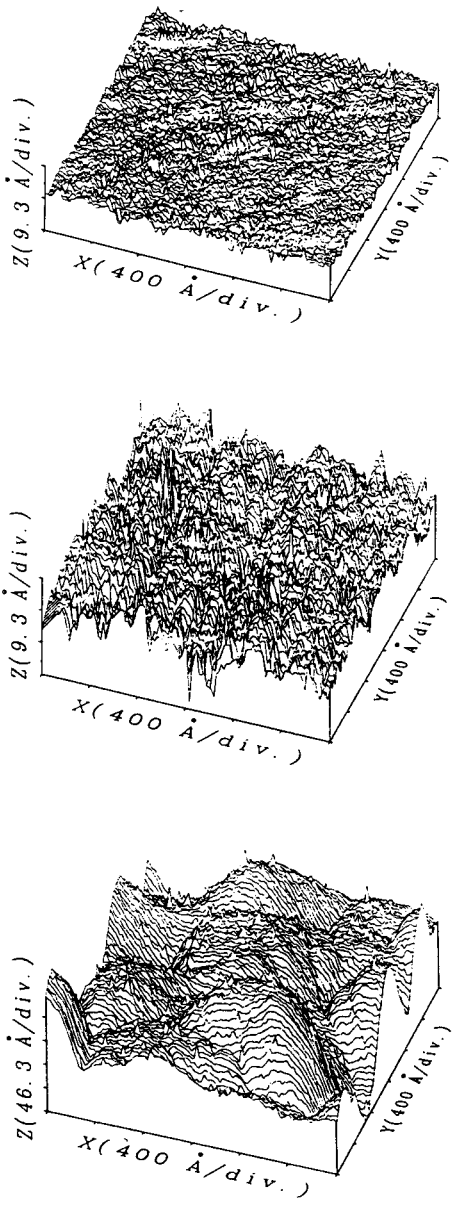

Fig. 16. STM image of a graphite surface after sputtering at room temperatuare with a flux of 6.9×10^{13} ions/cm^{2}s for 145 (a), 1450 (b), and 14500 s (c). This figure is reproduced from Eklund *et al.*, Ref. 82.

5.1.3. SiO_2

1994: Mayer *et al.*[83] studied the erosion of SiO_2 surfaces with 1 keV Xe ions. The surfaces were bombarded at an angle 55° with respect to normal with a flux of 3.2×10^{12} ions/cm^{2}s and fluences ranging from 2×10^{14}–8×10^{15} ions/cm^2. The samples were studied *it situ* with X-ray reflectivity and the growth exponent $\beta = 1$ was obtained from the dependence of the rms width on the amount removed (0.5–20 nm). Examination of the sample with AFM revealed a rippled topography (Fig. 17). Mayer *et al.* interpreted this within the context of a model based on curvature-dependent sputter yield variations, leading to features with preferred spatial frequencies in addition to a smaller scale stochastic roughness. The surface became smoother when irradiated with 1 keV He ions.

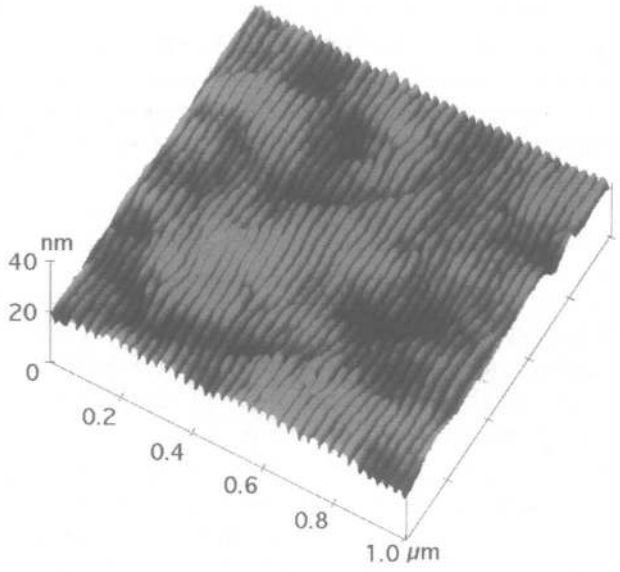

Fig. 17. 1 μm^2 AFM image of a Xe-sputtered SiO_2 film. This figure is reproduced from Mayer *et al.*, Ref. 83.

5.1.4. *Ge*

1994: Chason *et al.*[84] studied ion-beam erosion of Ge(001) surfaces with 1 keV Xe ions. The surfaces were bombarded at 150, 250 and 350°C at an angle 55° with respect to normal, along a ⟨110⟩ azimuth, with fluxes in the range 10^{12}–10^{13} ions/(cm^{2}s) and fluences ranging from 2×10^{14}–1.7×10^{17} ions/cm^2. The samples were studied *in situ* with X-ray reflectivity along a ⟨100⟩ azimuth, yielding precise values for the saturated rms widths as a function of sputter time. At 350° C, the surface was observed to roughen with a sublinear time dependence, but no value for β was reported. At 250° the surface roughened exponentially in time, while

at 150° the surface reach a saturated steady state roughness. The data were interpreted within the context of a competition between roughening processes due to both stochastic fluctuations and structure-dependent sputtering yields, and smoothing processes due to surface diffusion and viscous relaxation effects. The surface roughening observed at 350° was more consistent with predictions of nonequilibrium growth theories than that observed at lower temperatures. This is consistent with arguments put forward by Chason *et al.* that the viscous relaxation smoothing mechanisms (which are not included in the growth theories) become more dominant at the lower temperatures.

5.2. *Other studies*

1994: You and Nagy[85] carried out an oxidation–reduction study where the growth exponents was reported for the evolution of surface topology as a function of the number of oxygen–reduction cycles for a Pt(111) substrate. This case involved neither the addition nor removal of material, but rather a surface rearrangement with each cycle. The sample was studied *in situ* by means of X-ray reflectivity in an electrochemical environment, yielding $\beta = 0.38$ for 2–9 cycles. This corresponded to increase in the rms width from 0.6 to 1.2 nm.

6. Summary

Self-affine scaling is clearly observed for only a fraction of the deposition and erosion conditions which are experimentally possible. Nonetheless, it is an important fraction, since such experimental conditions allow for unique comparisons with theory. Let us now comment on the overall consistency of experimental results with the various predictions of nonequilibrium growth models.

Nonconservative film growth, described by the KPZ equation (See Table 1), is associated with the exponents $H = 0.385$ and $\beta = 0.240$. The value $H = 0.385$ is within experimental error of the roughness exponents reported for Ag/quartz at 77 K,[45] Au/Si(111) at 220 K,[74] Au/glass at 300 K[62] and ion-beam erosion of graphite at 300 K.[82] Of these, the two involving Au film growth yield growth exponents $\beta = 0.41 \pm 0.06$ which are clearly out of range of the KPZ prediction. The Au/glass films are moreover described by $H = 0.89$ for lateral length scales below 38 nm,[62] the range over which virtually all other experimental studies were carried out. No value for the growth exponent was reported for Ag/quartz at 77 K. A value for the dynamic exponent $z = H/\beta = 1.6$-1.8 was reported for ion erosion of graphite, which is consistent with the KPZ value.

Conservative models for nonequilibrium growth predict roughness exponents in the range $H = 0.67$–1 and growth exponents in the range $\beta = 0.2$–0.33 (Table 1). Approximately 90 % of the roughness exponents reported for the vapor-deposition systems fall in the range 0.7–1.0, and about half of the growth exponents for the corresponding systems are observed to be in the range 0.2–0.33. One half of the experimentally-observed growth exponents nonetheless fall outside of the range predicted by the MBE models, and half of these exceed the value $\beta = 1/2$, the maximum

value allowed under the assumption of stochastic roughening. In no case did ion erosion yield an exponent (either H or β) which was consistent with predictions of conservative growth models.

There are many potential explanations for the paucity of experimental reports yielding KPZ-type scaling behavior. The voids and overhangs associated with growth described by the KPZ model could produce physically unstable samples which collapse as they form, or decay shortly thereafter. This is in fact the case for Ag films deposited at 77 K,[68] a system which is potentially described by the KPZ exponents.[45] Another possible explanation for the relatively few reports of KPZ exponents is that many of the experimental techniques yield more precise values for higher values of H. Such systems may therefore be reported more frequently. Finally, many of the experimental studies described here have been driven by practical application: since MBE growth is of great technological interest, it has been extensively studied. Ion beam erosion of graphite at 300 K is the single experimental system to date whose scaling behavior is consistent with the KPZ equation. It is perhaps significant that in no case did an ion erosion experiment yield an exponent (either H or β) which was consistent with the conservative growth equations (Table 3). These systems, which exhibit relatively little surface diffusion, hold promise for future, fundamental investigations of KPZ-like behavior.

There is considerable overlap between experimental observation for the vapor-deposition systems and the predictions of the conservative growth models. Strict agreement within the error bars of any particular experimental study is nonetheless not observed with the various conservative models. The simple "pure diffusion" equation moreover yields exponents which agree with the collective experimental values as well as the more sophisticated MBE models. Two issues are perhaps important here. The first involves the propensity of growth exponents which are greater than the theoretically predicted values. This would indicate one or more roughening mechanisms are present in addition to stochastic roughening. Such mechanisms must ideally be included in considerations of film growth, as they have been for systems involving ion-beam erosion.[83,84] A second potentially important issue involves the formation of grains in the process of film growth. Microcrystalline grain formation is the rule, rather than the exception, in film growth. In at least one experimental system (Ag/quartz at 300 K)[73] the microcrystalline grains are observed to be on the same order as the coherence length for the roughness. It is striking that the latter system was well-described by scaling exponents which were relatively close to those predicted by models which completely neglect the presence of grain boundaries in either the film of the substrate.

As a final comment, we note that over 50 % of the experimental work reported here was published in the interval from January 1993 to August 1994. The pace of experimental work is clearly accelerating, and rapid advances in the field can be expected. Future developments notwithstanding, the experimental ability to systematically characterize random surface topology will remain a prime accomplishment of this field.

Acknowledgments

We gratefully acknowledge M. Siegert and M. Plischke for their careful reading of the first sections of the manuscript. This work was supported by the NSF grant# DMR9204022 and PRF grant#27498-AC5.

References

1. B. B. Mandelbrot, *The Fractal Geometry of Nature* (Freeman, New York, 1982).
2. J. Krim, D. H. Solina and R. Chiarello, *Phys. Rev. Lett.* **66**, 181 (1991).
3. J. H. Sikkenk, J. M. J. van Leeuwen, E. O. Vossnack, and A. F. Bakker, *Physica* **146A**, 622 (1987); J. H. Sikkenk, Ph.D. Thesis (R. U. Leiden, 1987), p. 81; see also J. H. Sikkenk, J. H. Hilhorst and A. F. Bakker, *Physica* **131A**, 587 (1985).
4. M. W. Mitchell and D. A. Bonnell, *J. Mater. Res.* **5**, 2244 (1990).
5. J. Krim, I. Heyvaert, C. Van Haesendonck and Y. Bruynseraede, *Phys. Rev. Lett.* **70**, 57 (1993).
6. Y.-L. He, H.-N. Yang, T.-M. Lu and G.-C. Wang, *Phys. Rev. Lett.* **69**, 3770 (1992).
7. M. A. Rubio, C. A. Edwards, A. Dougherty, and J. P. Gloub, *Phys. Rev. Lett.* **63**, 1685 (1989); V. K. Horvath, F. Family and T. Vicsek, *J. Phys.* **A24**, L25 (1991).
8. E. Bauer, *Z. Kirstallogr.* **110**, 3772 (1958).
9. T. Vicsek, *Fractal Growth Phenomena* (World Scientific, Singapore, 1989).
10. J. Krug and H. Spohn, in *Solids far from Equilibrium: Growth Morphology and Defects*, ed. C. Gordreche (Cambridge Univ. Press, Cambridge, 1991); P. Meakin, *Phys. Rep.* **235**, 191 (1994); *Surface Disordering: Growth, Roughening and Phase Transitions*, eds. R. Jullien, J. Kertesz, P. Meakin and D. E. Wolf (Nova Science, Commack, 1992).
11. G. Binnig, H. Rohrer, Ch. Gerber and E. Wiebel, *Appl. Phys. Lett.* **40**, 178 (1982); G. Binnig and H. Rohrer, *Helv. Phys. Act.* **55**, 726 (1982); G. Binnig, C. F. Quate and Ch. Gerber, *Phys. Rev. Lett.* **56**, 930 (1986).
12. P. Pfeifer, Y. J. Wu, M. W. Cole and J. Krim, *Phys. Rev. Lett.* **62**, 1997 (1989).
13. S. K. Sinha, E. B. Sirota, S. Garoff and H. B. Stanley, *Phys. Rev.* **B38**, 2297 (1988).
14. H.-N. Yang, T.-M. Lu and G.-C. Wang, *Phys. Rev. Lett.* **68**, 2612 (1992).
15. H. J. Ernst, F. Fabre, R. Folkerts and J. Lapujoulade, *Phys. Rev. Lett.* **72**, 112 (1994).
16. H. A. Atwater *et al.*, *Evolution of Surface and Thin Film Microstructure*, eds., *Mater. Res. Soc. Symp. Proc.* **280** (MRS, Pittsburgh, 1993).
17. J. Krim and J. O. Indekeu, *Phys. Rev.* **E48**, 1579 (1993). The roughness exponent has frequently been represented by α in the literature, and has also been represented by ζ, χ and h. It has been termed the "Hurst", or "Holder" exponent, as well as the "static" scaling exponent.
18. Ref. 1, p 264 and C14.
19. F. Family and T. Vicsek, *J. Phys.* **A18**, L75 (1985). See also *Dynamics of Fractal Surfaces*, eds. F. Family and T. Vicsek (World Scientific, Singapore, 1991).
20. M. Kardar, G. Parisi and Y.-C. Zhang, *Phys. Rev. Lett.* **56**, 889 (1986).
21. S. F. Wilkinson, *Proc. Roy. Soc.* (*London*) **A381**, 17 (1982).
22. J. Villain, *J. Phys. I* **1**, 19 (1991).
23. B. M. Forrest and L.-H. Tang, *Phys. Rev. Lett.* **64**, 1405 (1990).
24. Z. W. Lai and S. Das Sarma, *Phys. Rev. Lett.* **66**, 2348 (1991).
25. H. Yan, *Phys. Rev. Lett.* **68**, 3048 (1992); D. A. Kessler, H. Levine and L. M. Sander, *Phys. Rev. Lett.* **69**, 100 (1992).
26. M. Siegert and M. Plischke, *Phys. Rev.* **E50**, 917 (1994); M. Siegert and M. Plischke, *Phys. Rev. Lett* **73**, 1517 (1994).

27. M. D. Johnson, C. Orme, A. W. Hunt, D. Graff, J. Sudijono, L. M. Sander and B. G. Orr, *Phys. Rev. Lett.* **72**, 116 (1993).
28. P. Pfeifer and D. Avnir, *J. Chem. Phys.* **79**, 3558 (1983); see also D. Avnir, D. Farin and P. Pfeifer, *Nature (London)* **308**, 261 (1984).
29. J. M. Drake, P. Levitz and J. Klafter, *Israel J. Chem.* **31**, 135 (1991).
30. P. G. de Gennes, in *Physics of Disordered Materials*, eds. D. Adler, H. Fritzsche and S. R. Ovshinsky (Plenum, New York, 1985).
31. J. Frenkel, *Kinetic Theory of Liquids*, (Oxford Univ. Press, London, 1949); G. D. Halsey *J. Chem. Phys.* **17**, 520 (1949); T. C. Hill, *J. Chem. Phys.* **17**, 590 (1949).
32. E. Cheng and M. W. Cole, *Phys. Rev.* **B38**, 987 (1988).
33. M. Kardar and J. O. Indekeu, *Europhys. Lett.* **12**, 161 (1990); *Phys. Rev. Lett.* **65**, 663 (1990).
34. H. Li and M. Kardar, *Phys. Rev.* **B42**, 6546 (1990).
35. P. Pfeifer, J. Kenntner and M. W. Cole, in *Fundamentals of Adsorption*, eds. A. B. Mersmann and S. E. Sholl (Engineering Foundation, New York, 1991), p. 689.
36. A. V. Neimark, *Pis'ma Zh. Eksp. Teor. Fiz.* **51**, 535 (1990) [*JETP Lett.* **51**, 608 (1990)].
37. D. Avnir and M. Jaroniec, *Langmuir* **5**, 1431 (1989); M. Jaroniec, X. Lu, R. Madey and D. Avnir, *J. Chem. Phys.* **92**, 7589 (1990).
38. P. Pfeifer, in *Surface Disordering: Growth, Roughening and Phase Transitions*, eds. R. Jullien, J. Kertesz, P. Meakin and D. E. Wolf (Nova Science, Commack, 1992).
39. M. O. Robbins, D. Andelman and J. F. Joanny, *Phys. Rev.* **A43**, 4344 (1991).
40. A. Braslau, P. S. Pershan, G. Swislow and B. M. Ocko, *Phys. Rev.* **A38**, 2457 (1988).
41. M. Born and E. Wolf, *Principle of Optics* (Pergamon Press, Oxford, 1970).
42. J. Als-Nielsen, in *Handbook on Synchrotron Radiation*, Vol. 3 (North Holland, New York, 1991).
43. M. F. Toney and C. Thompson, *J. Chem. Phys.* **92**, 3781 (1990).
44. Ref. 13, Eqs. (4.41) and (4.42).
45. R. Chiarello, V. Panella, J. Krim and C. Thompson, *Phys. Rev. Lett.* **67**, 3408 (1991).
46. D. E. Savage *et al.*, *J. Appl. Phys.* **69**, 1411 (1991).
47. W. Weber and B. Lengler, *Phys. Rev.* **B46**, 7953 (1992).
48. G. Palasantzas, and J. Krim, *Phys. Rev.* **B48**, 2873 (1993).
49. C. Thompson, G. Palasantzas, Y. P. Feng, S. K. Sinha and J. Krim, *Phys. Rev.* **B49**, 4902 (1994).
50. R. Pynn, *Phys. Rev.* **B45**, 602 (1992).
51. S. Sinha *et al.*, unpublished.
52. M. G. Lagally, D. E. Savage and M. C. Tringides, in Procs. NATO Advanced Workshop on Reflection High Energy Electron Diffraction and Reflection Electron Imaging of Rough Surfaces, eds. by P. K. Larsen and P. J. Doba, *Series B*, **188**, 139 (1987).
53. I. K. Robinson, *Phys. Rev.* **B33**, 3830 (1990).
54. H. Luth, *Surfaces and Interfaces of Solids*, (Springer-Verlag, Berlin 1993), pp. 208-209.
55. Eq. (6) in Ref. 14.
56. H.-N. Yang, G.-C. Wang and T.-M. Lu, *Diffraction from Rough Surfaces and Dynamic Growth Fronts*, (World Scientific, Singapore, 1993).
57. B. J. Hinch and J. P. Toennies, *Phys. Rev.* **B42**, 1209 (1990); A. M. Lahee, J. R. Manson, J. P. Toennies and Ch. Woll, *Phys. Rev. Lett.* **57**, 471 (1986); B. J. Hinch, *Phys. Rev.* **B38**, 5260 (1987); A. Lock, B. J. Hinch and J. P. Toennies, in *Kinetics of Ordering and Growth at Surfaces*, ed. M. Lagally (Plenum, New York, 1990).
58. Ed. E. Hulpke, *Helium Atom Scattering from Surfaces* (Springer-Verlag, Berlin 1992), p. 15.
59. R. Wiesendanger, *J. Vac. Sci. Tech.* **B12**, 515 (1994).

60. S. Miller and R. Reifenberger, *J. Vac. Sci. Technol.* **B10**, 1203 (1992).
61. P. Herrasti, P. Ocon, P. Vazquez, R. C. Salvarezza, J. M. Vara and A. J. Arvia, *Phys. Rev.* **A45**, 7440 (1992); P. Herrasti, P. Ocon, R. C. Salvarezza, J. M. Vara, L. Vazquez and A. J. Arvia, *Electrochimica Acta.* **37**, 2209 (1992).
62. R. C. Salvarezza, P. Vazquez, P. Herrasti, P. Ocon, J. M. Vara and A. J. Arvia, *Europhys. Lett.* **20**, 727 (1992).
63. The fractal dimension in the publication is written as $D = 2 - H$, rather than $D = 3 - H$, since profiles embedded in two (rather than three) spatial dimensions are analyzed.
64. R. Messier and J. E. Yehoda, *J. Appl. Phys.* **58**, 3739 (1985); J. E. Yehoda and R. Messier, *Appl. Surf. Sci.* **22/23**, 590 (1985); R. Messier and R. C. Ross, *J. Appl. Phys.* **53**, 6220 (1982).
65. J. J. Friel and C. S. Pande, *J. Mater. Res.* **8**, 100 (1993).
66. D. J. Miller, K. E. Gray, R. T. Kampwirth, and J. M. Murduck, *Europhys. Lett.* **19**, 27 (1992).
67. D. J. Eaglesham and G. H. Gilmer, in *Surface Disordering: Growth, Roughening and Phase Transitions*, eds. R. Jullien J. Kertesz, P. Meakin and D. E. Wolf (Nova Science, Commack, 1992).
68. V. Panella and J. Krim, *Phys. Rev.* **E49**, 4179 (1994).
69. J. Krim and V. Panella, in *Characterization of Porous Solids II*, eds. F. Rodriguez-Reinoso *et al.*, (Elsevier, Amsterdam, 1991).
70. A. V. Neimark, *Phys. Rev.* **B50**, 15435 (1994).
71. J. Vrijmoeth, H.A. van der Vegt, J. A. Meyer, E. Vlieg and R. J. Behm, *Phys. Rev. Lett.* **72**, 3843 (1994).
72. I. Heyvaert, J. Krim, C. Van Haesendonck and Y. Bruynseraede, unpublished.
73. G. Palasantzas and J. Krim, *Phys. Rev. Lett.* **73**, 3564 (1994).
74. H. You, R. P. Chiarello, H. K. Kim and K. G. Vandevoort, *Phys. Rev. Lett.* **70**, 2900 (1993).
75. A. Iwamoto, T. Yoshinobu and H. Iwasaki, *Phys. Rev. Lett.* **72**, 4025 (1994).
76. J. Chevrier, V. Le Thanh, R. Buys and J. Derrien, *Europhys. Lett.* **16**, 737 (1991).
77. M. A. Cotta, R. A. Hamm, T. W. Staley, S. N. G. Chu, L. R. Harriott, M. B. Panish and H. Temkin, *Phys. Rev. Lett.* **70**, 4106 (1993).
78. W. M. Tong, R. S. Williams, A. Yanase, Y. Segawa and M. S. Anderson, *Phys. Rev. Lett.* **72**, 3374 (1994).
79. G. W. Collins, S. A. Letts, E. M. Fearon, R. L. McEachern and T. P. Bernat, *Phys. Rev. Lett.* **73**, 708 (1994).
80. G. S. Bales, R. Bruinsma, E. A. Eklund, R. P. Karunasiri, J. Rudnick and A. Zangwill, *Science* **249**, 264 (1990).
81. R. Bruinsma, in *Surface Disordering: Growth, Roughening and Phase Transitions*, eds. R. Jullien *et al.* (Nova Science, Commack, 1992).
82. E. A. Eklund, R. Brouinsma, J. Rudnick and R. S. Williams, *Phys. Rev. Lett.* **67**, 1759 (1991).
83. T. M. Mayer, E. Chason and A. J. Howard, *J. Appl. Phys.* **76**, 1633 (1994).
84. E. Chason, T. M. Mayer, B. K. Kellerman, D. T. McIlroy and A. J. Howard, *Phys. Rev. Lett.* **72**, 3040 (1994).
85. H. You and Z. Nagy, *Physica* **B198**, 187 (1994).